Available online at www.sciencedirect.com

ScienceDirect

Geochimica et Cosmochimica Acta 328 (2022) 58–75

Geochimica et Cosmochimica Acta

www.elsevier.com/locate/gca

A mechanistic investigation of the coral Mn/Ca-based trade-wind proxy at Kiritimati

Alice U. Chapman [a,*], Diane M. Thompson [a], Stephan R. Hlohowskyj [b,1], Jessica E. Carilli [c,2], Gwyneth Gordon [d], Tyler J. Goepfert [d], Hussein R. Sayani [e], Thomas M. Marchitto [f], Kim M. Cobb [e]

[a] *Department of Geosciences, University of Arizona, 1040 E. 4th Street, Tucson, AZ 85721, USA*
[b] *Department of Earth and Atmospheric Sciences, Central Michigan University, 1200 S. Franklin Street, Mount Pleasant, MI 48859, USA*
[c] *Scripps Institution of Oceanography, 9500 Gilman Drive, La Jolla, CA 92093, USA*
[d] *School of Earth and Space Exploration, Arizona State University, 781 E Terrace Mall, Tempe, AZ 85257, USA*
[e] *School of Earth and Atmospheric Sciences, Georgia Institute of Technology, 311 Ferst Drive, Atlanta, GA 30332, USA*
[f] *Institute of Arctic and Alpine Research, University of Colorado Boulder, 4001 Discovery Drive, Boulder, CO 80303, USA*

Received 3 September 2021; accepted in revised form 26 April 2022; Available online 4 May 2022

Abstract

Tropical Pacific trade-wind behavior is linked to the El Niño-Southern Oscillation and Pacific Decadal Variability, which modulate the rate of climate change. Despite their importance, high-resolution trade-wind observations span only the past 30–40 years and are too sparse to assess decadal wind variability and long-term trends. Previous work demonstrated that reef-building corals growing at the tropical Pacific island of Tarawa (2°N, 165°E) exhibit spikes in the manganese-to-calcium ratio (Mn/Ca) of their skeleton in response to a reversal of trade winds (i.e., westerly winds). Records of Mn/Ca from long-lived corals therefore hold great promise as indicators of past trade-wind variability. However, at other nearby islands with west-facing lagoons, there is a lag between westerly winds and coral Mn/Ca spikes and a significant difference in the magnitude of spikes between corals. To address uncertainties in how winds are recorded by coral Mn/Ca, we assess the reservoirs of Mn in the sediment, sediment pore spaces (porewater), and water column of Kiritimati's lagoon and inland lakes (1.9°N, 157.5°W). We find that insoluble dustborne Mn, once buried in lagoon sediments, becomes reduced and more soluble, leading to its accumulation in the sediment porewater. This Mn reservoir is then released into the water column when strong westerly wind events cause sufficient water-column mixing to reach lagoonal sediments. While this mechanism is consistent with what was previously proposed at Tarawa, the concentration of dissolved porewater Mn at Tarawa is nearly 20 times greater than at Kiritimati. We attribute this difference to the water depth of the sediment core from which porewater was sampled and the time elapsed between the most recent westerly wind event and core sampling, which both influence the "recharge time" of the porewater Mn reservoir. As such, lagoon bathymetry and morphology modulate lagoon water and sediment porewater Mn concentrations, which impact how westerly winds imprint their signal onto coral Mn/Ca. Armed with an improved understanding of the mechanism behind this coral Mn/Ca-trade wind relationship, we can better assess the reliability of this coral

* Corresponding author.
E-mail addresses: alicechapman@email.arizona.edu (A.U. Chapman), thompsod@arizona.edu (D.M. Thompson), Stephanh@email.arizona.edu (S.R. Hlohowskyj), jessica.c.carilli.civ@us.navy.mil (J.E. Carilli), gwyneth.gordon@asu.edu (G. Gordon), tyler.goepfert@asu.edu (T.J. Goepfert), hsayani@gatech.edu (H.R. Sayani), thomas.marchitto@colorado.edu (T.M. Marchitto), kcobb@gatech.edu (K.M. Cobb).
[1] Present address: Oak Ridge Institute for Science and Education, 1299 Bethel Valley Road, Oak Ridge, TN 37830, USA.
[2] Present address: Naval Information Warfare Center Pacific, San Diego, CA 92052, USA.

https://doi.org/10.1016/j.gca.2022.04.030

proxy through space and time and identify optimal sites for Mn/Ca-based wind reconstructions, paving the way for critical new insights into the role of winds in future climate change.

Keywords: Coral Mn/Ca; El Niño; Wind proxy; Manganese redox

1. INTRODUCTION

Tropical Pacific trade-wind behavior controls global climate by modulating sea-surface warming and subsurface ocean heat uptake on decadal and interannual timescales (England et al., 2014; Thompson et al., 2015). Interannual warming patterns in the Pacific can be attributed to El Niño-Southern Oscillation (ENSO), with wind behavior playing the key role of initiating anomalous sea-surface warming during El Niño events. The weakening of easterly trade winds allow intermittent bursts of westerly wind associated with Madden-Julian oscillation (MJO), the 40–50 day cycle of intraseasonal variability in atmospheric convection, to travel eastward as a trade-wind reversal event (Madden and Julian, 1971; Madden, 1986). Such abrupt, short-lived westerly wind events (WWEs) trigger a series of downwelling Kelvin waves that carry warm water eastward as they propagate across the equatorial Pacific (Kessler et al., 1995). WWEs are a fundamental component of the onset and maintenance of anomalous atmosphere and ocean conditions in the equatorial Pacific that are associated with an El Niño event, and are also thought to contribute to the classification of El Niño diversity (Vecchi and Harrison, 2000; Eisenman et al., 2005; Chen et al., 2015; Fedorov et al., 2015). This strong connection between trade-wind behavior and ENSO is also evident in global, atmosphere–ocean coupled climate models, where their skill in reproducing ENSO is contingent upon their ability to represent MJO and WWEs over the western Pacific (Shi et al., 2009; Seiki et al., 2011). In this way, there is much evidence for the inextricable link between trade-wind behavior and Pacific climate variability.

With uncertainty surrounding future El Niño behavior associated with global climate change, historical wind patterns that shed light on past El Niño behavior are key for understanding future climate variability. However, a continuous record of reliable historical wind observations in the tropical Pacific region only began in 1985, which is insufficient for the analysis of interannual, let alone decadal, variability (Chiodi and Harrison, 2017). Further, daily-resolved observational wind records do not capture the transient (sometimes on the order of hours) nature of westerly winds. Daily wind reanalysis data extend back to 1850 (i.e., 20th century reanalysis), simulated from sea-surface observations (e.g., sea level and temperature) using numerical weather prediction. However, these reanalysis products are still limited by the very few observations that exist prior to 1985 in this critical region. We must supplement these sparse wind observations with other reliable wind records to improve predictions of future climate change.

Corals act as high-resolution archives of surface ocean conditions due to their ability to grow quickly and continuously (e.g., 1–2 cm/year for massive Porites sp.). They exhibit sub-annual growth variability over centuries, with each added layer containing the geochemical signature of their surrounding environment, which allows for sub-annual climate reconstructions (Knutson et al., 1972; Lough, 2010; Saha et al., 2019). This is possible because of corals' tendency to incorporate certain isotopes, radionuclides, and trace metals into their skeletons as they grow, whose skeletal concentrations covary with changes in climate parameters (Shen, 1993; Thompson, 2022). By tracking the variability of these concentrations, it is possible to identify certain natural and anthropogenically-driven perturbations (e.g., Shen and Boyle, 1988).

One such trace metal is manganese (Mn), whose ratio to calcium (Mn/Ca) within the coral skeleton has diverse applications as an indicator of climate conditions. Historically, coral Mn/Ca has had site-specific applications as an indicator of vertical mixing (Shen and Sanford, 1990; Shen et al., 1991) and sediment loading from land-use change (Inoue et al., 2014) and riverine flood events (Lewis et al., 2018). Corals that live near the mouth of continental rivers are exposed to and incorporate dissolved metals (e.g., Mn) that have been released from fine-grained sediments in estuarine environments and transported via river flood plumes (Landing and Bruland, 1980; Shen et al., 1991). Other corals that live in coastal upwelling zones are subject to a flow of deep, nutrient-enriched and Mn-depleted waters, and thus have a Mn/Ca signature that reflects changes in upwelling intensity, with higher Mn associated with reduced upwelling (Shen and Sanford, 1990; Shen et al., 1991, 1992). More recently, coral Mn/Ca has shown promise as a new indicator of tropical Pacific trade-wind behavior in reef-building corals at the remote, equatorial Pacific atolls of Tarawa, Kiritimati, and Butaritari (Shen et al., 1992; Thompson et al., 2015; Sayani et al., 2021) (Fig. 1). Specifically, Mn/Ca spikes measured in corals that grow near west-facing lagoons correspond to WWEs that precede El Niño events. At such a distance from the continents, neither terrestrial runoff nor coastal upwelling are expected to contribute significantly to this coral Mn/Ca signal. While some remote equatorial islands are proximal to the zone of equatorial upwelling, weakened Walker circulation that accompanies El Niño events serves to dampen upwelling intensity and may thereby further increase surface Mn concentration when Mn/Ca spikes are observed in corals.

The proposed mechanism of this coral-based wind indicator at sites with large west-facing lagoons consists of five reservoirs of Mn: 1. dust, 2. sediment, 3. porewater, 4.

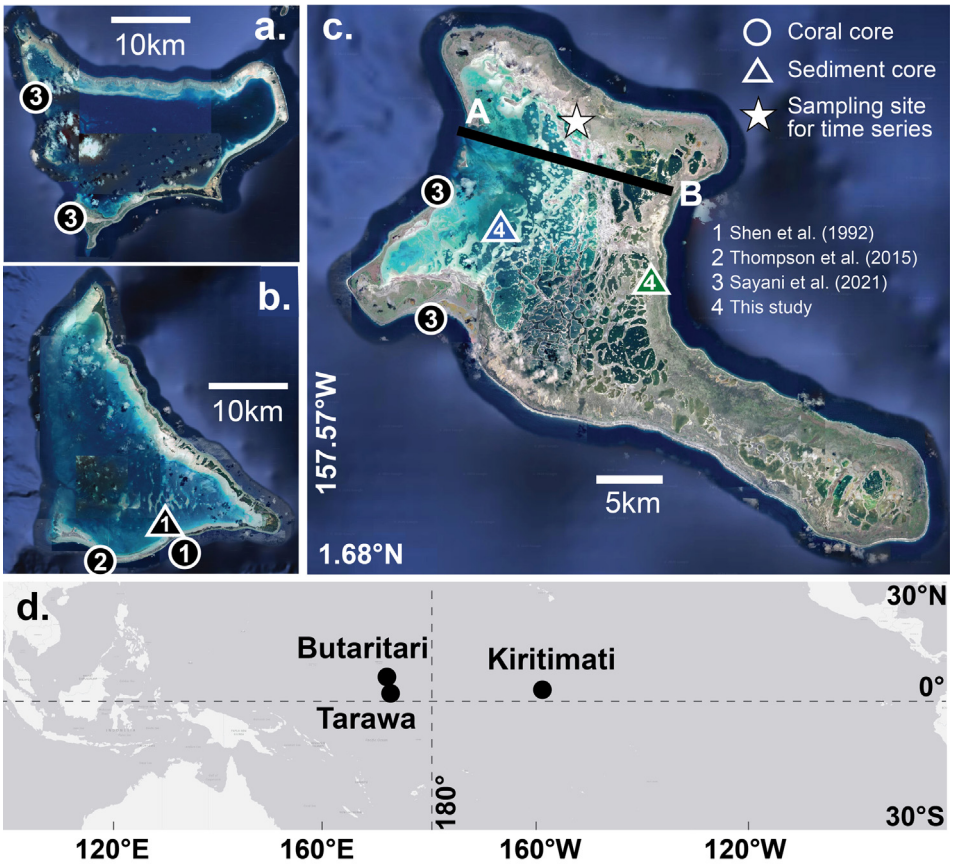

Fig. 1. Google satellite imagery of (a) Butaritari, (b) Tarawa, and (c) Kiritimati atolls, with (d) a map of the equatorial Pacific Ocean for context. Sites of previously analyzed coral (sediment) cores are indicated by black circles (triangles). Numbers correspond to studies: 1. Shen et al. (1992); 2. Thompson et al. (2015); 3. Sayani et al. (2021); 4. this study. Lagoon (blue; LAG20-C02) and lake (green; C22A, C22B) sediment cores analyzed in this study are marked by colored triangles, with colors corresponding to sediment and porewater Mn records in Fig. 5. The site from which lagoon water was collected weekly from December 2018 to April 2019 is indicated by a white star. Transect A-B is linked to the cross-section schematic in Fig. 2. Map data: GoogleMaps and Terrametrics (2020).

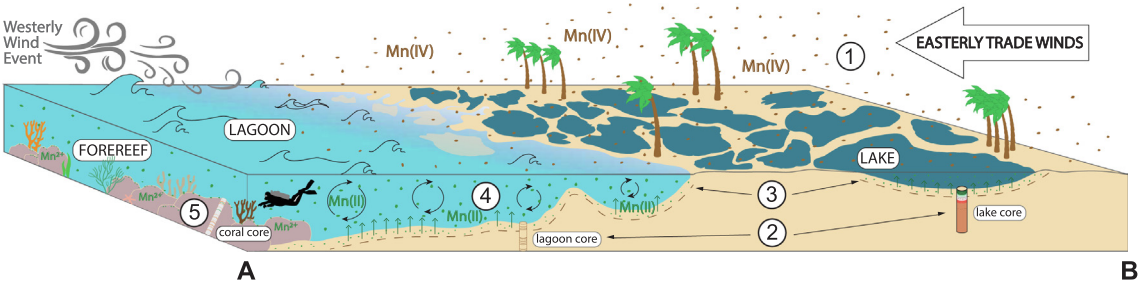

Fig. 2. Schematic of the coral Mn/Ca-based trade-wind proxy mechanism at Kiritimati atoll, adapted from the mechanism originally proposed at Tarawa atoll (Shen et al., 1992). This cross-section of Kiritimati is linked to transect A-B in Fig. 1. Steps 1-5 trace the Mn signal as it is transferred from the wind as dust (1), through the water column to the sediment (2), to the sediment porewater space (3), back into the water column (4) due to WWE-driven mixing, and to the coral (5).

seawater, and 5. coral (Fig. 2). Active dust deposition is considered the main source of Mn to remote islands such as Tarawa, Kiritimati, and Butaritari (Shen et al., 1992). For example, asymmetric lake basin profiles on Kiritimati provide evidence of significant dust deposition and accumulation at this site (Valencia, 1977). This Mn-laden dust releases particulate Mn oxides and oxyhydroxides (i.e., Mn(IV) form) within minutes after coming into contact with seawater (Statham and Chester, 1988), which then settle through the water column and are rapidly removed (scavenged) by advection and/or adsorption onto sinking particles (Statham et al., 1998). Over time, this particulate Mn(IV) is buried in lagoon sediments and diagenetically reduced to Mn(II) (i.e., the dissolved form favorable for coral uptake). The west-facing orientation of the lagoon shelters its waters from mixing by easterly trade winds, thus

allowing dissolved Mn(II) to accumulate in the interstitial porewater of the lagoon sediments. However, intermittent, strong bursts of westerly winds preceding El Niño events mechanically mix the west-facing lagoon's waters, remobilizing the dissolved Mn(II) stored in porewater below the sediment–water interface. This resuspended plume of Mn (II)-enriched water advects out over nearby corals and is subsequently incorporated into coral skeletons (in place of Ca(II)), leading to an increase in coral Mn/Ca (Fig. 2). This mechanism is specific to Mn and is contingent upon the unique combination of the following qualities, which are not possessed by any other trace metal: similar ionic radius to Ca(II) leading to lattice-bound incorporation into the coral skeleton, redox sensitivity, tendency to dissolve and migrate upwards in sediment porewater, and the ability to remain in a reduced state even after being reintroduced to the water column (Table S1).

This relationship between coral Mn/Ca, WWEs, and El Niño events has been reproduced at atolls with west-facing lagoons on either side of the date line, where WWEs occur prior to and during El Niño events. The link between Mn/Ca and WWEs was first discovered by Shen et al. (1992) at Tarawa atoll, an island in the Gilbert Island chain in the equatorial Pacific (1.5°N, 173°E, Fig. 1b), where WWEs tend to form early in the El Niño development stage. This study was further replicated and extended by Thompson et al. (2015) at Tarawa to reconstruct a century-long wind record, linking Mn/Ca-based wind variability to patterns of global warming. More recently, the Mn/Ca-WWE link was reproduced by Sayani et al. (2021) at two additional equatorial Pacific islands: Butaritari (3°N, 173°E) and Kiritimati (1.9°N, 157.5°W) (Fig. 1a,c).

Despite the reproducibility of this coral Mn/Ca-wind relationship at different islands, there are still a few key uncertainties that must be addressed before it can be applied more widely to coral records from other sites. First, while WWEs and coral Mn/Ca spikes are concurrent at Tarawa, there is a lag of approximately 1 year between them in the corals sampled at Butaritari and Kiritimati (Sayani et al., 2021). In addition, there is a difference in the magnitude of the spike between islands. These discrepancies merit an investigation of the various reservoirs of Mn in atoll systems that link coral Mn/Ca to WWEs.

To date, the proposed mechanism linking winds to coral Mn/Ca has not been tested beyond Tarawa (Shen et al., 1992). By analyzing the geochemistry of water, sediment, and porewater from the lagoon and lakes of Kiritimati atoll, we trace the step-wise transformation of Mn as it migrates between seawater, sediment, porewater, and coral. Our key objectives of this study are to:

1. Compare the Mn reservoirs that link coral Mn/Ca to westerly wind activity (i.e., lagoon sediments, porewater and seawater) at Kiritimati and Tarawa atoll.
2. Deconstruct the mechanism of Mn(II) accumulation in sediment porewater by analyzing the geochemistry of a Kiritimati lake as a case study.
3. Examine the spatiotemporal variability of lagoon and lake water Mn(II).

2. KIRITIMATI ATOLL: THE IDEAL TEST BED

Located in the central equatorial Pacific, Kiritimati has a unique set of properties that makes it the ideal place for investigating the mechanism of the coral Mn/Ca-based trade-wind indicator. Kiritimati has the greatest land area of any coral atoll on Earth (Morrison and Woodroffe, 2009), and an extensive network of interconnected, shallow lakes on the eastern side (Fig. 1). Finally, while the atoll experiences nearly constant 4 m/s southeast trade winds throughout the year (Valencia, 1977; Anderson et al., 2000), its large, west-facing lagoon (190 km^2) is subject to westerly wind-driven mixing during El Niño events.

Today, Kiritimati has a semi-arid environment due to its position about 400 km south of the average position of the Intertropical Convergence Zone (ITCZ), the zonal band of globally elevated precipitation (Anderson et al., 2000; Saenger et al., 2006; Higley et al., 2018; Wyman et al., 2021). Despite seasonal shifts in the ITCZ's meridional position that lead to an annual rainfall maximum of 4–6 mm per day in March-April (McGregor et al., 2013), Kiritimati receives an annual average of only 2 mm rainfall per day (Higley et al., 2018; Wyman et al., 2021), with an average precipitation-evaporation (P-E) balance of −2 mm/day (Schoonmaker et al., 1985). Nevertheless, local precipitation and sea level varies in accordance with ENSO cycles, with an increase in P-E balance and sea level of + 7 mm/day and 0.5 m, respectively, during an El Niño event (Schoonmaker et al., 1985; Woodroffe and McLean, 1998).

Kiritimati's lakes cover about one fourth of the island's land extent (Valencia, 1977) and range in area from 0.01 to 15 km^2 (Higley and Conroy, 2019). While human activity has altered the flow between certain lakes, some are naturally isolated from the lagoon, and others are connected via a complex system of tidal channels. Kiritimati experiences mixed, semidiurnal tides with a maximum range of 1.12 m, leading to changes in the water level and salinity of the lakes connected to the lagoon. Therefore, lake water levels are influenced by tidal fluctuations and the island's geomorphology. The lakes' variable degrees of connectivity with the lagoon results in their large salinity range, from brackish (15 ppt) and marine (35 ppt) around the perimeter of the island, to hypersaline (200 + ppt) in the island's interior (Saenger et al., 2006). This layout is a remnant of the mid-Holocene, when sea level was up to 0.25 m higher (Woodroffe et al., 2012); the hypersalinity of some interior lakes is a product of continuous evaporation of trapped seawater from this time (Saenger et al., 2006) (Fig. 6). Most lakes also contain a thick, benthic layer of finely-laminated microbial mats that generate heat through respiration, resulting in an inverse thermal stratification (warmer water at depth) in these lakes (Saenger et al., 2006; Schmitt et al., 2019; Chen et al., 2021). The juxtaposition of Kiritimati's lagoon and lakes is advantageous for tracking the Mn signal as it moves between reservoirs. Though not directly involved in the coral Mn/Ca-wind mechanism, the lakes play an important role in understanding the mechanism by allowing the isolation of certain steps. For example, the lakes receive the same Mn-laden dust input as the

lagoon; however, the lakes are not as readily mixed by WWEs compared to the lagoon due to their smaller fetch. The lakes are therefore treated as a case study, with the Mn behavior of their water, sediments, and porewater providing insight into the link between the lagoon's counterpart reservoirs. Together, Kiritimati's location in the trade-wind belt, its large west-facing lagoon, and its many lakes make it an ideal test bed for this in-depth examination of the coral Mn/Ca-wind mechanism.

3. MATERIALS AND METHODS

3.1. Sample collection and preparation

We collected water samples and sediment cores from the main lagoon and lakes of Kiritimati throughout the day over the course of a 2-week period from November 30 to December 11, 2018. The analysis of these samples not only helps us understand the behavior of Mn as it moves through the island's various reservoirs, but also demonstrates how the island system has changed over time when compared against samples collected over the past decades (Table S2).

3.1.1. Water sampling

We targeted specific lakes for water sampling based on previously-collected salinity data (Saenger et al., 2006), accessibility of roads, and potential for resampling during future field seasons. The selected lakes, which range from brackish to hypersaline, provide an even representation of the salinity spectrum of these lakes (Fig. 6). Due to the shallow nature of many lakes, we sampled subsurface water at up to 0.5 m depth.

We collected subsurface seawater samples throughout the lagoon as well to examine the spatial variability of lagoon water chemistry. We determined sampling sites in the main lagoon based on accessibility via boat; many areas of the lagoon were too shallow to be accessed without causing damage to existing coral reefs. We collected seawater samples at 1 m depth below the surface with a Van Dorn Water Sampler and measured bathymetry concurrently. At the deepest part of the lagoon (near the mouth), we collected samples at 2 m, 4 m, and 8 m depths to generate a chemical depth profile.

At each lake and lagoon site, water sampling consisted of collecting and filtering sub-surface water samples with 0.45 μm nylon filters into separate bottles (with no head space) for future analysis of trace metals (cations), anions, and salinity. To compare water chemistry with physiochemical and environmental conditions, we used a portable Yellow Springs Instruments (YSI) Pro Plus Multiparameter Sonde to measure temperature, dissolved oxygen content, conductivity, total dissolved solids, salinity, pH, and oxidation reduction potential (ORP), referred to hereafter in our data as Eh. Measurement uncertainty for salinity is reported to be 1.0% (YSI Incorporated, 2018). As with sample collection, we made YSI measurements throughout the day.

We used the same water sampling scheme (without YSI measurements) for the 2018–2019 time series: a local collaborator collected seawater from the lagoon on a weekly basis for 5 months immediately after the 2018 field season (i.e., between December 2018 to April 2019; Fig. 1). These samples were not acidified until shipped back to the Tropical Climate and Coral Reefs Laboratory at the University of Arizona in Tucson, AZ, up to 6 months after the sampling date. We compared this 2018–2019 time series with an earlier seawater Mn(II) time series spanning March-August 2016 (i.e., the tail end of the 2015–2016 El Niño event). This earlier time series consisted of weekly seawater samples collected by a local collaborator. While the sampling location changed week-to-week and the exact coordinates are unknown, we are confident that these seawater samples are from the main lagoon. Due to the uncertainty of sample location, we compare the average Mn(II) concentration from these samples against the lagoon seawater Mn(II) concentration from December 2018 to April 2019 (i.e., a period without WWEs). Finally, we resampled water from a subset of lakes and lagoon sites in January 2020 using the same water sampling scheme.

We brought lake and lagoon water samples back to the University of Arizona and stored them at 5 °C (40°F) until analysis. Upon return, we acidified water samples for trace-metal analysis to pH 2 with ultrapure (Fisher Optima) nitric acid.

3.1.2. Sediment and porewater sampling

We cored a subset of the lakes from which water was sampled, and collected duplicate cores at sites with favorable conditions; we based these decisions on spatial distribution and accessibility, prioritizing sites that had been previously cored for sake of comparison (Saenger et al., 2006; Higley et al., 2018). We cored lagoon and lake sediments using an Aquatic Research Instruments Universal Gravity corer with a 50 cm-long polycarbonate core tube (10 cm diameter). Resulting cores ranged in length from 10 to 50 cm. We collected lake sediment cores from the deepest section of the lake (~1 m), and the gravity corer was easily pushed through the soft, gelatinous algal layers. We collected lagoon sediment cores in 0.5–1.5 m water depth in areas free of coral rubble and other large pieces of carbonate. In most cases, the coarse texture of the sediment required the person coring to use a twisting technique when using the gravity corer. Core tops were always recognizable and recovered, and we extruded the upper 8–13 cm (lagoon) and 3–7 cm (lake) of sediment cores at 2–5 mm resolution within 1–4 h of coring and stored them in Whirl-Pak bags. The remainder of the cores were preserved in their coring tubes by inserting floral foam to absorb excess water. For some lagoon and lake cores, we measured the redox potential (Eh) and pH of each extruded layer by inserting a Hach Eh/pH probe into each Whirl-Pak in such a way that the entirety of the probe's sensors was submerged in the sediment and porewater slurry. Probe uncertainty is reported as ± 20 mV for Eh, and ± 0.1 for pH (Hach, 2016). We transported the extruded sediment samples, as well as the remainder of the cores, back to the University of Arizona in a liquid nitrogen-charged dewar and kept them at −80 °C until we prepared them for porewater extraction. We documented each core

photographically in the field, and we described the lake core's distinct layers as they were extruded. The location of the sediment cores whose sediment and porewater we analyzed for this study are shown in Fig. 1.

We extracted porewater from each extruded layer of one lagoon (LAG20-C02) and 2 lake cores (C22A, C22B, Fig. 1) in an anoxic glovebox using a Rhizon soil moisture sampler with 0.12–0.18 μm pore size from Rhizosphere Research Products (Seeberg-Elverfeldt et al., 2005; Shotbolt, 2010). We extracted ~ 2 mL of porewater from each 2–5 mm extruded depth interval, which is sufficient for trace element analysis.

We dried the sediment samples remaining after porewater extraction at 40 °C, then heated to 500 °C for 14 h to remove all organic matter; the percent weight difference is thus expressed as the weight percent of organic matter content contained in each extruded lagoon and lake sediment sample (Heiri et al., 2001). We estimated the uncertainty of percent organic matter content in lagoon and lake sediments (±3.58%; Fig. 4) from the average standard deviation of corresponding depth intervals from two replicate cores (LAG20-C01 and LAG20-C02). We then treated these combusted samples with a multi-step digestion consisting of hydrofluoric, nitric, and hydrochloric acids (Gordon et al., 2009) and diluted the remaining liquid to 2% HNO_3. A procedural blank for sediment digestion had a Mn concentration that was 3.93% of average sediment Mn concentrations.

3.2. Trace-metal analysis of water, porewater, and sediment samples

We diluted water and porewater samples 10-fold, and digested sediment samples 150-fold before analyzing their major, minor, and trace element composition via Quadrupole Inductively Coupled Plasma-Mass Spectrometer (ICP-MS; Thermo Fisher Scientific iCAP Q) at Arizona State University's Metals, Environmental and Terrestrial Analytical Laboratory (ASU METAL). We also analyzed standard reference materials NASS-5 (open ocean), CASS-5 (near-shore), and SLEW-3 (estuarine) in parallel with samples for the purpose of quantifying accuracy and analytical uncertainty of low-level Mn measurements. Over the course of four different analytical runs, the measured value of Mn in NASS-5 was 1.196 ± 0.320 ppb (1σ, $N = 21$), compared to the known value of 0.919 ± 0.057 p pb (Miller and Wu, 1998). The measured value of Mn in CASS-5 was 2.599 ± 0.172 ppb (1σ, $N = 22$), compared to the known value of 2.620 ± 0.200 ppb (National Research Council of Canada, 2010a). The measured value of Mn in SLEW-3 was 1.564 ± 0.079 ppb (1σ, $N = 22$), compared to the known value of 1.610 ± 0.220 ppb (National Research Council of Canada, 2010b). We calculated analytical uncertainty by taking the root-sum-square of both reproducibility (i.e., precision) and bias (i.e., accuracy) of all three external standards, after Szpak et al. (2017) (Table S3). These are therefore conservative

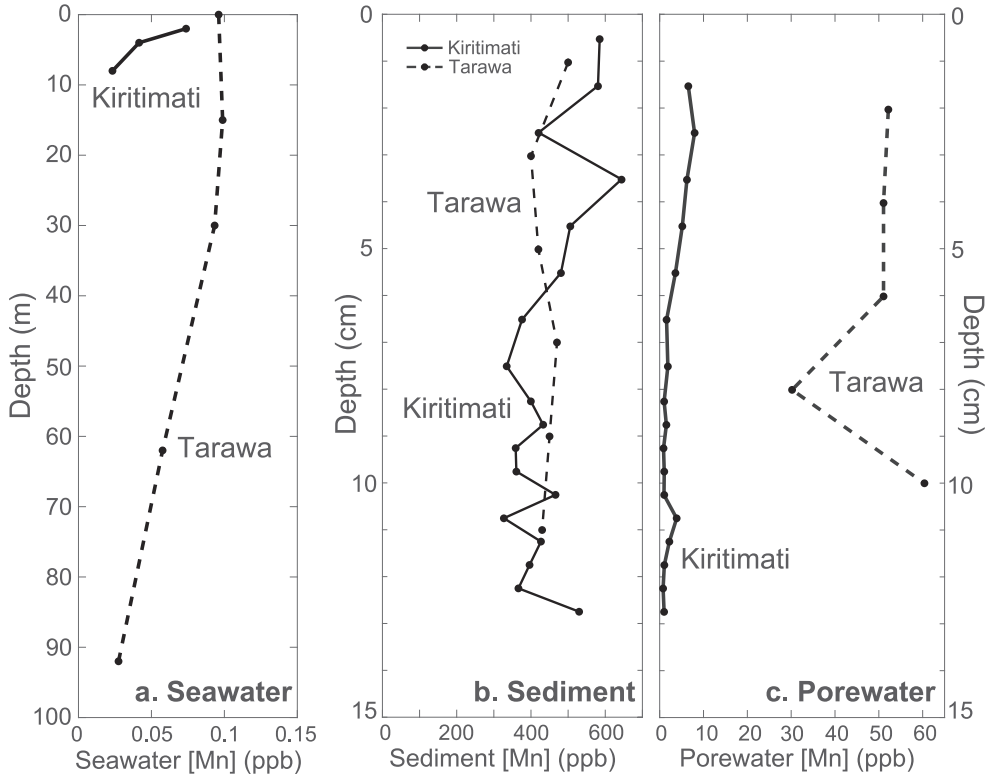

Fig. 3. Depth profiles of (a) water, (b) lagoon sediment, and (c) corresponding sediment porewater Mn concentration at Kiritimati (solid line) and Tarawa (dotted line; Shen et al., 1992). Analytical uncertainty of seawater Mn at Kiritimati is ± 0.320 ppb (1σ; determined from NASS-5) and ± 0.172 ppb (1σ; determined from CASS-5) for Kiritimati sediment and porewater Mn. At Tarawa, analytical uncertainty was only reported for seawater measurements (± 10%; Shen et al., 1992).

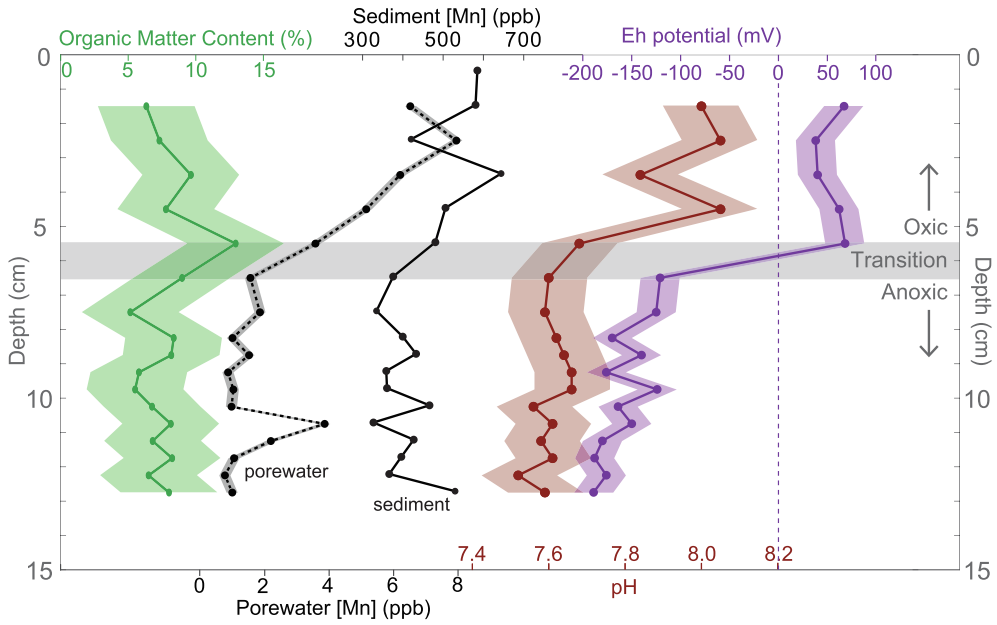

Fig. 4. Depth profiles of Kiritimati lagoon sediment Mn(IV) concentration (solid black) and percent organic matter content (green), as well as porewater Mn(II) concentration (dotted black), Eh potential (purple), and pH (maroon) at corresponding depth. Analytical uncertainty for each field is plotted: ± 3.58% organic matter content, ± 0.172 ppb (1σ; determined from CASS-5) sediment and porewater Mn concentration, ± 20 mV for Eh, and ± 0.1 for pH. Due to figure scale, analytical uncertainty of sediment Mn concentration is not visible. The vertical dotted purple line indicates 0 mV, where Eh potential switches from positive (oxic) to negative (anoxic), and the gray shaded horizontal bar indicates the depth at which this transition zone occurs in the sediment core.

estimates of analytical uncertainty. For example, while reproducibility for NASS-5 (seawater standard with the lowest Mn concentrations) is comparable to previously published work, the standard uncertainty is elevated by the increased bias of these low-concentration samples (bias = 0.277 ppb; 1σ reproducibility = 0.161 ppb). We report analytical uncertainties for each sample type based on the external standard whose average Mn concentration is closest to that of the sample type: NASS-5 for samples with [Mn] < 1.196 ppb, CASS-5 for samples with [Mn] ≥ 2.599, and SLEW-3 for samples with [Mn] between NASS-5 and CASS-5.

3.3. Wind records

We analyzed three observational wind records and two reanalysis zonal wind data sets with variable spatial and temporal resolution to compare against coral Mn/Ca and seawater Mn records at Kiritimati. Wind speed and direction parameters are recorded at Kiritimati's Cassidy International Airport at 3-hourly resolution and have been available since 2012 (rp5.ru, 2020). For sake of comparison against other records, we calculated the daily average of this 3-hourly wind record for the 2012–2018 interval. We also compared this 3-hourly wind record to averaged daily wind at Cassidy Airport over the 1996–2015 period, which we downloaded from the Biological and Chemical Oceanography Data Management Office (BCO-DMO). We calculated the zonal wind component from wind speed and direction parameters using trigonometry. We also downloaded daily zonal wind observations from the nearest Tropical Atmosphere-Ocean/Triangle Trans-Ocean Buoy Network (TAO/TRITON) buoy (270 km due east of Kiritimati at 2°N, 155°W) from the NOAA Pacific Marine Environmental Laboratory Global Tropical Moored Buoy Array. Finally, we downloaded daily reanalysis zonal wind data from National Centers for Environmental Prediction-National Center for Atmospheric Research Climate Data Assimilation System 1 (NCEP-NCAR CDAS-1; Kalnay et al. (1996)) for 1°N, 157.5°W and monthly observational zonal wind data from the International Comprehensive Ocean-Atmosphere Data Set (ICOADS; Freeman et al. (2017)) for a 10°x10° region around Kiritimati.

In the interest of comparing wind behavior between Kiritimati and Tarawa, we downloaded daily zonal wind observations from 2015 to 2020 and 1990 to 1995 recorded at the TAO/TRITON buoys nearest Kiritimati and Tarawa (2°N, 165°E), respectively. The Kiritimati and Tarawa TAO/TRITON wind records begin in 1991 and 1990, respectively; both records contain significant temporal gaps (Fig. S1).

Almost all working definitions of WWEs (also called westerly wind bursts, or WWBs, in the literature), were developed by analyzing zonal wind behavior in the western equatorial Pacific (Harrison and Giese, 1988; Giese and Harrison, 1991; Delcroix et al., 1993; Hartten, 1996; Verbickas, 1998;Eisenman et al., 2005). These definitions are all slightly different, consisting of some combination of wind speed, duration, and in some cases regional extent. The application of these definitions to the westerly winds

experienced at Kiritimati, however, results in much fewer WWEs, and most notably, no defined WWEs during the strong 2015–2016 El Niño event. Harrison and Vecchi (1997) do not limit their definition of WWEs to the western equatorial Pacific, but this definition considers zonal wind anomalies instead of absolute wind speed (as in Harrison and Giese, 1988; Giese and Harrison, 1991; Verbickas, 1998; Eisenman et al., 2005). Actual westerly winds, not mere westerly anomalies (e.g., weakening easterly winds) are required to set off the chain reaction that is at the core of this coral Mn/Ca-based trade-wind indicator. As such, it is clear that the existing definitions of WWEs are not suitable for the identification of noteworthy westerly winds at Kiritimati. We propose a new definition for WWEs that are experienced east of the date line and, more specifically, at Kiritimati. Westerly winds of a WWE are herein classified as having speeds at or greater than 2 m/s for a period of 2 or more days. By applying this definition to the TAO/TRITON (2°N, 155°W buoy) daily wind observations from July 1991 to June 2020, we find that Kiritimati has experienced 15 WWEs since July 1991, with an average wind speed and duration of 3.6 m/s and 3.4 days, respectively. In addition, according to our new definition, Kiritimati experienced 7 WWEs during the 2015–2016 El Niño event.

3.4. Calculation of minimum wind speed required for porewater resuspension

Due to Kiritimati and Tarawa's lagoon morphology and the predominant southwesterly winds experienced at both locales during WWEs, fetch lengths are obstructed by land on the perimeter of the lagoon and are reduced compared to what would be expected in an open ocean setting (Fig. S2). Therefore, we calculated the effective fetch according to Carper and Bachmann (1984). To calculate the minimum wind speed necessary for vertical mixing in the water column to reach the sediment–water interface at various depths, we related effective fetch to the wave period and wavelength as in Carper and Bachmann (1984) and Arfi et al. (1993), while assuming that wind speed stayed constant over a period of 1 h. Since each WWE has a unique direction, we calculated the zonal component of each WWE exceeding the wind speed threshold at Kiritimati and Tarawa and marked them in Fig. S1. While these calculated minimum wind speeds represent what is necessary for vertical mixing to reach the bottom of the lagoon, we view them as thresholds for porewater resuspension at the core sites.

It is worth noting that while this coral Mn/Ca proxy focuses on WWEs, it is possible that other extreme events that involve strong winds such as tropical cyclones could lead to lagoon mixing, porewater remobilization, and ultimately manifest in the coral record as a Mn/Ca spike. However, such events are exceedingly rare within 5° north and south of the equator. Between 1981 and 2011, only one tropical cyclone has formed within 1° latitude of Kiritimati, and only two events with a maximum intensity of Tropical Storm has formed within 1° latitude of Tarawa (Arthur and Woolf, 2013).

3.5. Bathymetry of Kiritimati's main lagoon

We used a Garmin ECHOMAP Plus 72sv, fixed to the bottom of the outrigger on a ~ 4.5 m fishing boat, to make sonar depth measurements every 20–30 seconds along tracklines parallel and perpendicular to a line spanning the mouth of the lagoon. We then corrected these depth measurements for tidal fluctuations. Depth measurements were limited due to the lagoon's shallow nature and were extended using FIJI software to create additional approximate tracklines based on satellite image analysis of the main lagoon (Fig. S3). First, we assigned color scale values from known lagoon depths (measured in the field) to create a calibration curve ($r^2 = 0.85$), including shallowest and deepest points measured. Then, we drew 16 east–west and 8 north–south transects across the lagoon of the Kiritimati satellite map. For each transect, we extracted colorscale values of 15–25 distinct points along the transect and converted to depth values using the calibration curve. The number of points selected varied depending on how many color (depth) changes there were to capture along the transect. We transferred these transect points to Geographic Information Systems software (QGIS) and, together with the bathymetric points measured in the field, created a digital elevation model of the lagoon via the Inverse Distance Weighting method of interpolation. This method best interpolates evenly-distributed points, and gives more weight to points that are closest when predicting a depth, which is appropriate for the gradual depth changes in Kiritimati's lagoon. For any given point in the lagoon, depth was highly correlated within a 500 m radius, and more weakly correlated (if at all) at a greater distance. This is because the eastern section of the lagoon contains a complex system of broad tidal flats, shoals, peninsulas, reefs, and islands, whose transition from the deeper areas is relatively abrupt. Therefore, we used a radius of 500 m for interpolation so as not to smooth over these geomorphological characteristics of the lagoon.

4. RESULTS

4.1. Comparison of Kiritimati and Tarawa Mn reservoirs

Side-by-side comparisons of water, sediment, and porewater Mn concentrations at Kiritimati and Tarawa reveal similarities for all but the porewater Mn(II) reservoir. At an average of 0.08 ppb, the surface seawater Mn(II) concentration of Kiritimati's main lagoon is comparable to that of Tarawa's main lagoon (Shen et al., 1992) (Fig. 3a). Kiritimati's lagoon sediment Mn(IV) concentration is also comparable to that of Tarawa, with an average of 466 ppb (Fig. 3b). This sediment Mn(IV) concentration is almost four orders of magnitude greater than that of seawater at both Kiritimati and Tarawa. While both locales have lagoon sediment porewater Mn(II) concentrations less than that of their sediment counterparts, their individual porewater Mn(II) values are very different. With an average of 49 ppb, Tarawa's porewater Mn(II) concentration is more than an order of magnitude greater than that of Kiritimati (2.8 ppb) (Fig. 3c).

The redox transition depth and organic matter content of sediments also differ between sites. The transition from oxic to anoxic environment in Tarawa's lagoon sediment core was reported to be within 2 cm of the surface, and the sediments contained an average of 1% organic matter (Shen et al., 1992). At Kiritimati, the oxic-anoxic transition of the sediment core was measured by ORP to be at about 5 cm, and the sediments contained an average of 7.6% organic matter (Fig. 4). The depth profile of Kiritimati lagoon sediment shows that porewater Mn(II) concentration, Eh, and pH are all elevated at less than 5 cm depth (Fig. 4). Porewater Mn(II) concentration is strongly correlated with Eh and pH (r = 0.86 & 0.88, respectively, $p < 0.05$, $N = 17$), as well as with sediment Mn(IV) concentration and percent organic matter content ($r = 0.53$ & 0.20, respectively, $p < 0.05$, $N = 17$).

4.2. Kiritimati Lagoon and Lake Comparison

The average Mn(II) concentration of water samples collected from 43 of Kiritimati's lakes is 0.18 ppb, which is 2.25 times greater than that of the lagoon (0.08 ppb). Lake sediment Mn concentration is comparable to that of the lagoon, and more than 3 orders of magnitude greater than the Mn concentration of the overlying water column (Fig. 5a). The lake sediment core exhibited significant variability of Mn(IV) concentration downcore, however, with a range of 500–1100 ppb. With an average of 10.48 ppb, the porewater Mn(II) concentration of the lake is about 4 times greater than that of the lagoon (Fig. 5b), and almost 2 orders of magnitude greater than the Mn(II) concentration of lake water. On average, lake sediments are 31.8% organic matter, which is about 4 times more than lagoon sediments (7.6%). This discrepancy can be attributed to most of Kiritimati's lakes having a thick unit of finely laminated microbial mats that grows at the sediment–water interface, unlike the lagoon (Higley et al., 2018; Schmitt et al., 2019).

4.3. Spatial variability of dissolved manganese in Kiritimati's lake and lagoon water

Kiritimati's lagoon and lakes have spatially variable Mn (II) concentration. Kiritimati's lakes contain an average of 0.18 ppb of Mn(II) and range from 0.05 to 0.76 ppb, whereas the main lagoon contains an average of 0.08 ppb Mn(II) and has a narrower range of 0.01–0.45 ppb (Fig. 6). In the case of the lakes, the concentration of Mn (II) is positively correlated with salinity (r = 0.306, $p < 0.05$, N = 43) and negatively correlated with pH ($r = -0.168$, $p < 0.05$, N = 43); a negative correlation between salinity and pH has been demonstrated by previous work (Saenger et al., 2006). These relationships do not hold for lagoon waters, where Mn(II) concentration is only very weakly positively correlated with salinity and pH ($r = 0.005$, $p < 0.05$, $N = 24$ for both).

The lagoon has variable bathymetry, reaching depths of up to 10 m, with two main channels on either side of Cook Island, which lies at the center of the mouth connecting the lagoon to the open ocean. The Mn(II) that reaches forereef corals is presumed to pass through these channels. While the Mn(II) concentration of lagoon water is not correlated with depth, the greatest concentration of Mn(II) (0.45 ppb) is found near the southern channel of the lagoon mouth (Fig. 6).

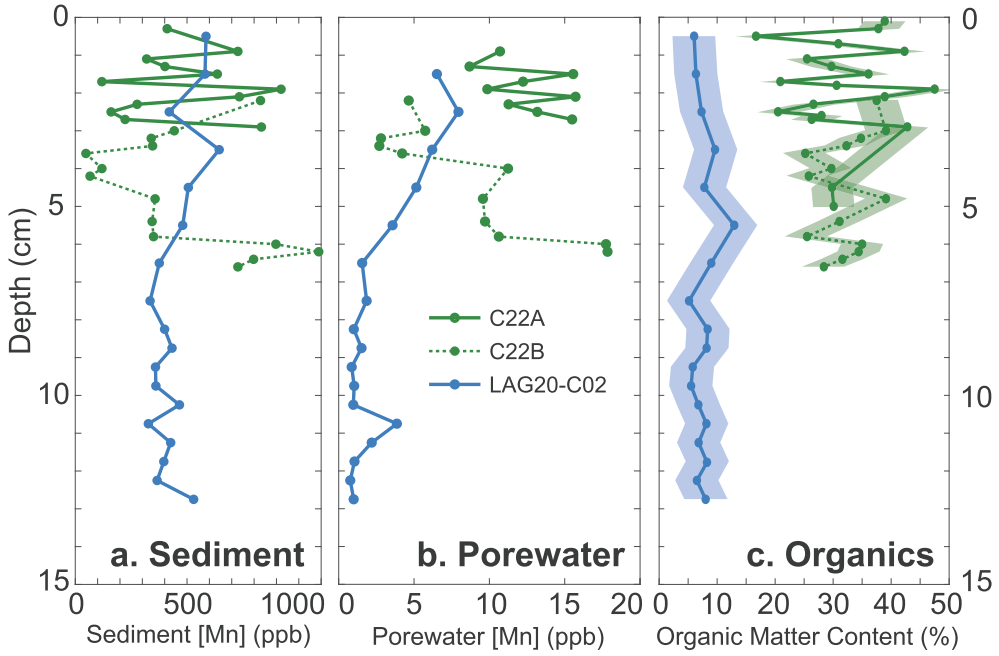

Fig. 5. Depth profiles of (a) sediment Mn(IV) concentration, (b) porewater Mn(II) concentration, and (c) sediment organic matter content of two replicate lake cores (solid green = C22A; dotted green = C22B) and a lagoon core (blue; LAG20- C02) from Kiritimati. Uncertainty of lake and lagoon sediment and porewater sample analyses is ± 0.172 ppb (1σ; determined from CASS-5) and ± 3.58% for lagoon and lake sediment organic matter content. Due to figure scale, analytical uncertainty of sediment and porewater Mn is not visible.

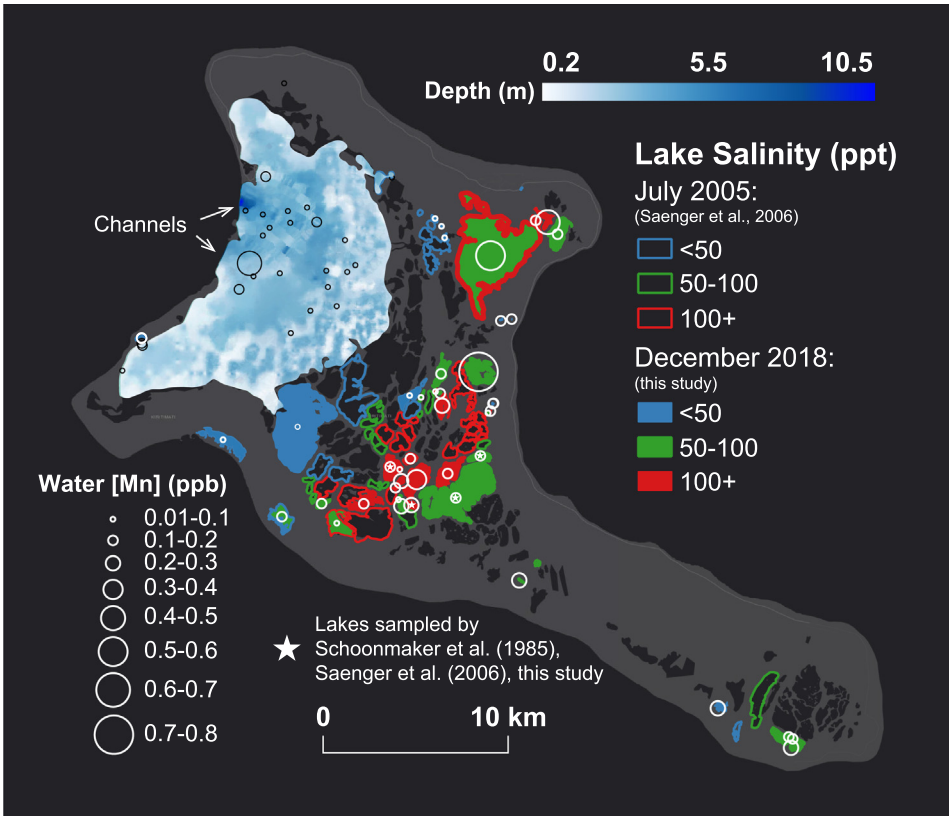

Fig. 6. Map of Kiritimati with lakes shaded (December 2018, this study) or outlined (July 2005, Saenger et al. (2006)) according to salinity category (i.e., less than 50 ppt in blue, 50-100 ppt in green, greater than 100 ppt in red). White (black) circles mark locations where water was sampled from the lakes (lagoon) in December 2018, with sizes corresponding to Mn(II) concentration measured, ranging from 0.01 to 0.8 ppb. Measurement uncertainty of salinity is ± 1.0% and analytical uncertainty of Mn concentration is ± 0.320 ppb for lagoon water samples (1σ; determined from NASS-5) and ± 0.172 ppb for lake water samples (1σ; determined from CASS-5). Small white stars mark the four lakes that were sampled by this study, Saenger et al. (2006), and Schoonmaker et al. (1985). Bathymetric digital elevation model of the lagoon, developed by applying the Inverse Distance Weighting method of interpolation to measured and estimated points, shows a range of depth from 0.2-10.5 m. Depths measured in the field by sonar and additional transects and points created for interpolation are detailed in Fig. S3.

4.4. Westerly wind events at Kiritimati

Due to its location east of the date line (i.e., farther away from where WWEs originate), Kiritimati experiences westerly winds that are weaker and less frequent than those experienced by equatorial islands located west of the date line. Furthermore, these westerly winds cannot be identified in all wind records; the temporal and spatial resolution of the wind record determines whether or not WWEs, let alone westerly winds, are captured. For example, westerly winds at Kiritimati associated with the strong 2015–2016 El Niño event were not apparent in monthly ICOADS data, but were reflected in 3-hourly and daily wind observations from the island and the nearby TAO/TRITON buoy, respectively, as well as in daily NCEP-NCAR CDAS-1 reanalysis data (Fig. S4). A further comparison between the Cassidy International Airport wind observations and the daily TAO/TRITON buoy wind record reveals a 1–5 m/s offset between the two records, which demonstrates that Kiritimati experiences weaker easterlies and stronger westerlies compared to the buoy located 270 km to the east (Fig. S4). For this reason, this study utilizes the 3-hourly (and daily-averaged) wind record from Cassidy International Airport, supplemented by the daily TAO/TRITON buoy data prior to 2010.

4.5. Temporal variability of dissolved manganese in Kiritimati's lagoon

The time series of Mn(II) concentration from weekly-sampled lagoon water spanning March-August 2016 and December 2018 to April 2019 reveal different Mn(II) concentrations between the two periods. The March-August 2016 record is at the tail end of the 2015–2016 El Niño event, while the December 2018 to April 2019 record is during a period of no WWEs (Fig. 7). With an average of 0.30 ppb, seawater collected during March-August 2016 has a Mn(II) concentration about 7 times greater than seawater measured between December 2018 and April 2019 (0.043 ppb) (Fig. 7).

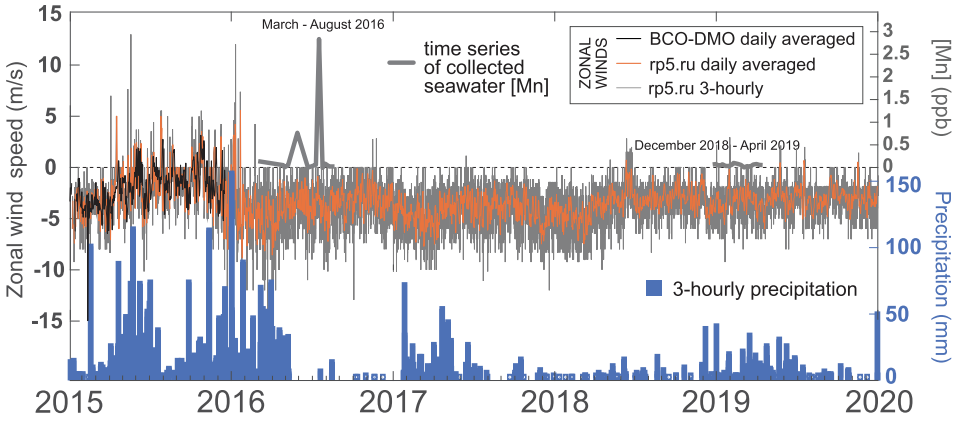

Fig. 7. Time series of lagoon water Mn(II) concentration from March-August 2016 and December 2018 to April 2019 (thick gray line) with zonal wind data calculated from wind direction and speed recorded at Cassidy International Airport, Kiritimati every 3 hours (thin gray line) and averaged daily by two separate sources (BCO-DMO in black; rp5.ru in orange). 3-hourly precipitation data (blue bars) were also collected from Cassidy International Airport. Analytical uncertainty for lagoon water samples is ± 0.320 ppb (1σ; determined from NASS-5). Horizontal dotted gray line indicates 0 m/s zonal winds, and positive (negative) zonal winds are westerly (easterly). Lagoon water collected between December 2018 and April 2019 was sampled from the site indicated by a white star in Fig. 1.

5. DISCUSSION

5.1. A mechanistic comparison between Tarawa and Kiritimati

At Kiritimati, measured coral Mn/Ca background values are 2–3 times greater than those of Tarawa, and Mn/Ca spikes are up to 14 times the magnitude of Tarawa's (Sayani et al., 2021). This suggests that there is a fundamental difference in the geochemistry and/or established Mn transfer pathway between the water, sediment, and porewater reservoirs of these two islands.

At Kiritimati, the water and sediment Mn reservoirs demonstrate the same step-wise accumulation that was observed at Tarawa (Fig. 3). Depth profiles of seawater Mn(II) concentration at both islands exhibit the behavior of a scavenged element, which corroborates the particle reactive nature of Mn in the water column, with its short, 5- to 25-year surface ocean residence time (Klinkhammer and Bender, 1980; Landing and Bruland, 1980; Chen and Wu, 2019). The Mn surface maxima at both islands is also characteristic of remote waters, where the main Mn input is atmospheric due to the islands' isolation from the continents (Shen et al., 1991) (Fig. 3a). This is illustrated in the surface Mn concentration of 0.085 ppb compared to up to 0.3 ppb off the California coast (Landing and Bruland, 1980). The slight difference in Mn(II) concentration of surface seawater at Tarawa and Kiritimati (~0.01 ppb; Fig. 3) can most likely be attributed to the difference in depth and environment where the samples were taken (i.e., shallow lagoon at Kiritimati vs. open ocean just off the coast of Tarawa). The similarity between the water Mn reservoirs of both islands is also reflected in their sediment Mn concentrations. The comparable Mn concentration of Tarawa and Kiritimati lagoon sediments is in line with the fact that both islands are coral atolls and thus have sediments composed of predominantly calcium carbonate sand and very little organic matter (Shen et al., 1992) (Fig. 3b).

The most striking difference between Kiritimati and Tarawa is the 18-fold difference in porewater Mn concentration (Fig. 3c). In the following sections, we evaluate the possible explanations for this stark contrast, including: the organic matter content of sediments, the hydraulic and concentration gradients between sediment porewater and the overlying water column, the timing of sampling of Kiritimati and Tarawa sediment cores with respect to WWEs, and the depth at which these cores were taken.

5.1.1. The role of organic matter in porewater Mn(II) accumulation

Under low Eh and pH conditions in the anoxic zone of the Kiritimati lagoon sediment core analyzed in this study (LAG20-C02, Fig. 4), Mn(II) is more common than manganese oxides and oxyhydroxides (i.e., Mn(IV)) (Burdige, 1993). The production of carbon dioxide within these sediments is likely responsible for decreases in pH of the porewater. As oxygen becomes depleted, however (likely due to a combination of diffusion and respiration), the sediments transition to anoxia at about 5 cm in the case of LAG20-C02 (Fig. 4). Within the anoxic zone, both nitrate and manganese oxides are thermodynamically-favored terminal electron acceptors, resulting in denitrification and manganese reduction, respectively (Burdige, 1993). By acting as an oxidant of organic matter, manganese oxides (particulate Mn(IV)) in sediments are reduced to Mn(II), which increases their solubility and releases free and/or organically-complexed ions into the porewater. We suspect that through this reduction–oxidation cycle, Mn(II) accumulates in lagoon sediment porewater at both Tarawa and Kiritimati.

The porewater and sediment Mn depth profiles in LAG20-C02 look very different from ideal profiles presented in the literature (Froelich et al., 1978; Burdige,

1993). Based on the thermodynamic ordering of electron acceptors and diffusion, one would expect a well-developed solid Mn oxide peak just above the oxic-anoxic transition in the sediments (i.e., redox boundary) and a lack of dissolved Mn(II) above this boundary. In theory, any Mn(II) that diffuses upward– due to a hydraulic gradient, wave pumping (Rodellas et al., 2020), or because of a concentration gradient resulting from an excess of Mn(II) production at depth (Boyle, 2001; Froelich et al., 1978) would oxidize upon contact with oxygen, forming the peak of solid-phase Mn above the redox boundary. Such a clear peak is not evident in LAG20-C02. While there is a relative peak at about 3.5 cm depth, it is not as pronounced as would be expected from earlier work in pelagic sediments (Fig. 4 vs. Froelich et al. (1978), Fig. 18)). These idealized profiles are based on pelagic sediments, however, which do not experience frequent changes in redox boundary location, allowing distinct solid-phase Mn peaks to develop. In shallow, coastal environments, however, bioturbation resulting from benthic infaunal activity is more intense compared to deeper pelagic sediments, which can lead to a "mosaic of biogeochemical microenvironments" (Burdige, 1993) in surficial sediments and a co-occurrence of both oxic and anoxic processes. In this way, bioturbation in LAG20-C02 could explain the observed peak in dissolved Mn(II) near the sediment–water interface.

While bioturbation could lead to the excavation of deeper sediments, placing Mn(II)-rich porewater at a shallower depth than the measured redox boundary (based on ORP), it does not explain why Mn(II) does not reoxidize in surficial sediments and also remains in its reduced form when it is resuspended into the water column. Despite Mn(II) oxidation being thermodynamically favored at atmospheric oxygen levels, the activation energy for this oxidation reaction is high, and can be a relatively slow process (Gounot, 1994). Furthermore, by measuring fluxes of dissolved manganese across the sediment–water interface via chamber incubation experiments, Pakhomova et al. (2007) found that the rate of Mn(II) oxidation is slower than the rate of its release from sediments. In addition, sunlight has been shown to prevent the re-oxidation of Mn(II), and also induces the reduction of MnO_2 by dissolved organic compounds in surface waters, thereby maintaining the reservoir of Mn(II) that is so vital for phytoplankton survival (Sunda et al., 1983; Sunda and Huntsman, 1994; Chen and Wu, 2019). These processes make it possible for resuspended (released) Mn(II) to remain in reduced form under oxic open-ocean conditions for up to a week (Tebo, 1991). A shallow, coastal lagoon environment is likely to experience more bacteria-mediated oxidation than an open-ocean environment, leading to a comparatively shorter residence time of dissolved Mn(II) (Tebo, 1991; Pakhomova et al., 2007). However, this demonstrates that the Mn(II) residence time in Kiritimati's sediments and lagoon water is on the order of days, giving it ample time to reach nearby forereef corals.

The accumulation of Mn(II) in porewater via oxidation of sedimentary organic matter is reinforced by a comparison between lake and lagoon geochemistry at Kiritimati. Despite having comparable average sediment Mn concentrations, the lake and lagoon (Fig. 1c green and blue triangles, respectively) have very different sediment porewater Mn(II) concentration and organic matter content (Fig. 5). The lake's porewater Mn concentration is about 4 times greater than that of the lagoon (Fig. 5b), and almost 2 orders of magnitude greater than the Mn concentration of lake water. While the organic matter percentage varies with depth, lake sediments contain on average 4 times more organic matter than lagoon sediments (Fig. 5c). Lake sediments therefore contain more organic matter to be oxidized, but the same amount of MnO_2, which we assume is the primary oxidant of organic matter after oxygen (and possibly nitrate) in these sediments. Organic matter oxidation via manganese reduction does not appear to be restricted by MnO_2, however, since the concentration of Mn(II) in lake sediment porewater is also elevated compared to the lagoon (Fig. 5b). While the redox potential of the lake's porewater was not measured, we hypothesize that the oxic-anoxic transition in lake sediments would be much shallower than that of lagoon sediments. Not only are Kiritimati's lakes more geographically isolated from WWE-driven mixing compared to the lagoon, the microbial mats that cap the lake sediments may prevent oxygen from penetrating deep into the sediments, and/or require greater wind strength to disturb sediments and to remobilize a similar flux of Mn as in the lagoon. Bubbles of pungent hydrogen sulfide released from the sediment–water interface when disturbed further support a shallow transition to an anoxic or sulfate-reducing environment (Valencia, 1977; Arp et al., 2012; Schneider et al., 2013; Schmitt et al., 2019; Chen et al., 2021). These microbial mats could also serve to trap dissolved Mn(II) in surficial sediments and promote shallow porewater Mn accumulation. Together, the increased organic matter content, shallow anoxic environment, and relatively undisturbed nature of the sampled lake sediments lead to elevated lake porewater Mn(II) concentration compared to lagoon sediments.

While the concentration of Mn(II) accumulated in the porewater of lake sediments was originally presumed to reflect that of lagoon sediment porewater prior to WWE-triggered remobilization, we find that the lakes' high organic matter content (i.e., microbial mats) plays a significant role as well. This precludes the use of the lakes as a true pre-mixing analog, though this analysis of lake water, sediments, and porewater has helped clarify the role of organic matter in porewater Mn(II) production and accumulation, a crucial component of the mechanism linking coral Mn/Ca and WWE behavior.

Based on our understanding of the role of sedimentary organic matter in the production of dissolved Mn(II), the organic matter content of Kiritimati and Tarawa lagoon sediments could potentially lead to the observed discrepancy in porewater Mn(II) concentration. However, despite having a greater organic matter content of 7.6%, Kiritimati lagoon sediments actually have a *lower* porewater Mn(II) concentration compared to Tarawa's lagoon sediments, which are 1% organic matter (Fig. 3). This suggests that there is at least one other force at play that is strong enough to counteract this difference in organic matter content to produce the 18-fold greater porewater Mn concentration at Tarawa compared to Kiritimati.

5.1.2. Tidal pumping

It is worth noting that there are other physical forces besides wind-driven mixing that can lead to porewater fluxes. Rodellas et al. (2020) discuss the hydraulic gradient and wave/tidal pumping as forces that could influence porewater fluxes in a lagoon environment. A change in the hydraulic gradient can control the movement of porewater and can be brought on by a change in water depth. For example, a decrease in lagoon water depth may lead to an increased hydraulic gradient, which could then induce the upward advection of porewater. Kiritimati and Tarawa have tidal ranges of 1.12 m and 2.25 m, respectively, which results in a greater change in lagoon water depth at Tarawa compared to Kiritimati. Based on Rodellas et al. (2020)'s findings, this stronger hydraulic gradient at Tarawa compared to Kiritimati would drive greater porewater flux activity, which contradicts Tarawa's elevated porewater Mn(II) concentration. Again, this suggests that there is yet another force controlling the porewater Mn reservoir, and that tidal pumping plays a secondary role.

5.1.3. "Recharge" time of porewater Mn

Another possible explanation for this discrepancy in porewater Mn(II) concentration is a difference in WWE intensity and/or frequency experienced at Kiritimati and Tarawa, and how these WWEs translate to porewater flux. Porewater fluxes are significantly higher during windy periods due to locally-generated wind-driven mixing that drives the circulation of lagoon waters through surficial sediments (Rodellas et al., 2020). With 3,300 km between them, it is expected that Kiritimati and Tarawa would experience different WWEs, and therefore different intensities of wind-driven mixing. In fact, Kiritimati experiences less frequent WWEs (4 WWBs from 1991 to 2020) compared to Tarawa (31 WWBs from 1990 to 2020), when using the Harrison and Vecchi (1997) definition to analyze wind records from TAO/TRITON buoys closest to Kiritimati and Tarawa.

While there is a notable discrepancy in overall WWE activity experienced at the two islands, the precise timing of WWEs with respect to when the sediment cores were taken, and the depths at which these cores were taken, prove to be more significant. First, differences in westerly wind speeds and effective fetch at the core sampling sites at Kiritimati (average 4.53 m/s and 4.45 m, respectively) and Tarawa (average 6.94 m/s and 6.38 m, respectively) lead to differences in the depth reached by wind-driven mixing (Fig. S2). At Kiritimati, we collected the lagoon sediment core (LAG20-C02) at a depth of 1 m, which translates to a minimum wind speed of 2.4 m/s necessary for mixing to reach the bottom of the lagoon and possibly resuspend porewater into the water column. At Tarawa, where the sediment core was taken at 4 m depth (Shen et al., 1992), southwesterly winds with a speed of at least 6.7 m/s are required to reach the bottom of the lagoon. Since we calculated minimum wind speeds for southwesterly winds and the available wind records are zonal, this means that WWEs of slightly lesser strength captured in zonal wind records could still reach the bottom of the lagoon, due to the trigonometric relationship between true wind direction and the zonal and meridional components. Calculating the zonal component yields a minimum westerly wind speed of 1.7 m/s at Kiritimati and 4.8 m/s at Tarawa. By treating these zonal wind speeds as a threshold for porewater flux, we can assume that sediment and porewater samples were collected at both Tarawa and Kiritimati during a period of time when winds were not strong enough to induce porewater resuspension (Fig. S1). The most recent WWE at Tarawa that led to porewater resuspension was on November 22, 1990, approximately 8 months before the sediment core was sampled by Shen et al. (1992) on July 18, 1990. At Kiritimati, a gust of southwesterly wind strong enough to trigger porewater resuspension took place on June 19, 2018, which is just less than 6 months prior to when we sampled LAG20-C02 on December 10, 2018. Therefore, a possible explanation for Tarawa's elevated porewater Mn(II) concentration is that Tarawa's sediment porewater had more time (i.e., 2 months longer) to "recharge" with Mn(II) prior to being resuspended compared to Kiritimati's sediment porewater.

Nevertheless, it is unlikely that a difference of 2 months for time elapsed between porewater resuspension and core sampling could lead to an 18-fold difference in porewater Mn(II) concentration between the two sites. Another possible explanation for the greater porewater Mn accumulation in Tarawa sediments is that at Tarawa, there is a weaker concentration gradient of Mn(II) between porewater of the top sediment layer and bottom lagoon water. While we do not know the Mn concentration of Tarawa lagoon waters, we can infer that it is greater than Kiritimati's lagoon waters due to the higher level of human activity at Tarawa (Shen et al., 1992). Since the diffusion of Mn(II) from porewater is controlled by the concentration difference between porewater and bottom water (Pakhomova et al., 2007), this weaker concentration gradient at Tarawa could lead to more Mn(II) trapped in the porewater reservoir.

In all likelihood, it is a combination of the aforementioned forces that leads to the elevated porewater Mn concentration at Tarawa compared to Kiritimati. While the organic matter content of sediments and the hydraulic and concentration gradients between sediment porewater and the overlying water column all play a role, we conclude that the main driver of the two islands' different porewater Mn(II) concentrations is the amount of time between core sampling and the most recent porewater resuspension event, which is based on WWE strength and the vertical reach of wind-driven mixing (i.e., Kiritimati vs. Tarawa core depths).

5.2. Temporal variability of Mn(II) in Kiritimati's lagoon and lakes

A preliminary time series of lagoon water Mn(II) concentration spanning March-August 2016 and December 2018 to April 2019 shows that there is a relationship between the occurrence of WWEs and the level of lagoon water Mn concentrations. While there were no WWEs during the March-August 2016 sampling period, it directly follows a period of observed WWEs associated with the 2015–2016 El Niño event, whose wind speeds exceeded

the threshold required for wind-driven mixing to reach sediments and induce porewater flux (Fig. 7, Fig. S1). On the other hand, the December 2018 to April 2019 sampling period does not overlap with or follow any WWE occurrences, which likely explains why the 2016 seawater samples have a mean Mn(II) concentration that is 7-fold that of the samples collected in 2018–2019 (Fig. 7). In addition to wind activity, precipitation patterns could also impact lagoon water Mn(II) concentration, either through rainwater dilution or terrestrial runoff-related trace-metal input. However, the large spikes in lagoon water Mn(II) concentration observed in 2016 occurred during a period of little to no precipitation; similarly, the rainfall that Kiritimati received during the 2018–2019 sampling period did not lead to any significant spikes in water Mn(II) concentration. The lack of dilution effect from rainwater may be explained by the lagoon's constant seawater exchange with the open ocean. The lack of trace-metal input from terrestrial runoff may be attributed to the very low Mn content of Kiritimati's soils. With an average of less than 1 mg/kg (or ppm) (~20 nmol/mol), soils cannot be expected to be a significant source of soluble Mn to water during large precipitation events (Morrison and Woodroffe, 2009). We therefore conclude that WWE activity and resulting porewater resuspension is the main driver of the temporal variability of Mn(II) in Kiritimati's lagoon. While we do not have an earlier time series of lagoon water Mn(II) that spans the WWEs of the 2015–2016 El Niño event, we see that Mn(II) in the lagoon remains elevated up to a year after WWEs are experienced by Kiritimati's lagoon. Perhaps this sustained state of elevated lagoon water Mn(II) plays a role in the lag time between coral Mn/Ca spikes and WWEs as observed by Sayani et al. (2021).

Although lake water samples have not been continuously collected over time, it is likely that lake water Mn(II) concentration, which is positively correlated with salinity, would exhibit temporal variability that is more responsive to precipitation events. This can be expected due to Kiritimati's semi-arid climate, and because the water chemistry of its isolated, shallow, hypersaline lakes are known to be very sensitive to the hydrologic balance of inputs and outputs, most notably evaporation/precipitation, sea level variability, and groundwater flow (Saenger et al., 2006; Higley et al., 2018; Higley and Conroy, 2019). We can piece together a record of temporal changes in salinity at select lakes by comparing salinity values measured in early December 2018 and January 2020 (this study), as well as measurements made in summer 2005, 1983, and spring/fall 1970 by Saenger et al. (2006), Schoonmaker et al. (1985), and Valencia (1977), respectively (Table S2). This comparison demonstrates the sensitivity of Kiritimati's lakes to precipitation. On November 26, 2018, Kiritimati received 37 mm of rainfall, which was just 4 days before water samples were collected from lakes. In contrast, there was no significant rainfall event in the months prior to the collection of water samples from the same 20 lakes in early January 2020. This difference in precipitation is reflected in the lakes' ionic composition, with 80% of the lakes having up to 65% greater salinity in 2020 compared to 2018 (Table S4). Of the 28 lakes that were sampled in both 2018 and 2005, 68% had a greater salinity in 2005 (Saenger et al., 2006). While we do not have precipitation data for 2005, greater salinity during this time suggests that Kiritimati had not received significant precipitation in the days to weeks prior to sampling in June-July 2005. To further illustrate the diluting effect that precipitation has on Kiritimati's lake chemistry, lake water samples collected during the very strong 1982–1983 El Niño event by Schoonmaker et al. (1985) had 43–75% lower salinity compared to that of corresponding lakes in 2005 and 2018 ($N = 4$; marked by stars in Fig. 6). With sea level increasing by ~ 0.5 m during this El Niño event, this lake water dilution could have been from a combination of heavy rainfall and/or an influx of seawater from the lagoon; in fact, the two lakes that exhibited the largest change in salinity are located closer to the lagoon (Fig. 6). Finally, the only lake that was sampled by all four studies had 157% greater salinity in 1970 compared to 1983, 2005, 2018, and 2020 (Valencia, 1977), which can be explained by the dry conditions experienced at Kiritimati due to the moderate La Niña event in 1970 (Fig. 3 of Saenger et al., 2006). Overall, by using salinity as an analog for lake water Mn(II) concentration (due to their strong correlation), we can infer that temporal variability in Mn(II) concentration in Kiritimati's lakes is linked to precipitation patterns and lagoon water intrusion from localized sea level rise.

5.3. Spatial variability of Mn(II) in Kiritimati's lakes and lagoon

The significant, positive correlation between salinity and Mn(II) concentration of Kiritimati's lakes implies that their spatial variability is linked as well (Fig. 6). The main hydrologic inputs are precipitation and groundwater intrusion, while evaporation serves to remove water and concentrate the ions contained in these closed-basin lakes (Valencia, 1977; Higley et al., 2018; Higley and Conroy, 2019). The most isolated lakes, located inland on the island's eastern side, therefore have the greatest salinity and water Mn(II) concentration. These inland lakes are the most cut off from hydrologic inputs such as seawater inflow and freshwater lenses, which would lower salinity and Mn(II) concentration (Anderson et al., 2000; Saenger et al., 2006). Lakes located progressively farther away from the interior of the island and in closer proximity to the lagoon (to the west) or eastern coast have lower salinity and Mn(II) concentration. This implies that these lakes are receiving more hydrologic input while maintaining the same outputs, thus diluting both the salinity and Mn(II) concentration of the lake water.

Unlike Kiritimati's lakes, the spatial variability of the lagoon's water Mn(II) concentration is not significantly correlated with salinity. Due to its connection to the open ocean, the lagoon is frequently flushed out and circulated, making the spatial Mn(II) concentration comparatively more homogeneous. This relative chemical homogeneity of the lagoon is reflected by the narrow range in water Mn(II) concentration compared to that of the lakes, almost 40% narrower, despite the lagoon's depth variability (up to 10.5 m, Fig. 6). One area of the lagoon whose Mn(II)

concentration deviates the most from this chemical homogeneity is at the mouth of the lagoon, where two channels north and south of a small island (Cook Island) connect the lagoon to the open ocean (Fig. 6). In general, sampling sites near the southern channel of the lagoon mouth have greater Mn(II) concentration compared to those near the northern channel (Fig. 6). While it is possible that the channeling of water from inside the shallow lagoon towards the relatively deep (8–10 m) mouth leads to an accumulation of Mn(II) in the water column, it does not explain the differences between north and south channels.

One possible explanation for this behavior is the timing of water sampling with regard to tides. Sites at the northern end of the lagoon mouth were sampled during a flood tide (low to high tide), whereas most sites at the southern end (including the site with highest Mn(II) concentration) were sampled during an ebb tide (high to low tide). A flood tide would carry the relatively Mn-depleted open ocean's water into the lagoon, in effect diluting the Mn(II) concentration of the lagoon, whereas an ebb tide would lead to a channeling effect, bringing the lagoon's Mn-enriched water together at the "bottleneck" of the lagoon mouth. Therefore, sampling near the northern channel during the flood tide and near the southern channel during the ebb tide could have led to lower and higher measured Mn(II) concentrations, respectively.

A second plausible explanation is that the two channels have different flow rates. The northern channel's frequent dredging history led Valencia (1977) to conclude that the northern channel experiences a faster sedimentation rate compared to the southern channel. This implies that water flows more slowly through the northern channel, allowing more sediment to settle out of the water column. This is corroborated by the northern channel's slightly greater width compared to the southern channel (1.40 km vs. 0.96 km). The relatively faster flow rate through the southern channel implies greater turbulence of the water column, perhaps leading to further resuspension of Mn-enriched sediment porewater. This suggests that lagoon morphology likely plays a role in controlling the Mn(II) concentration of the water column, and thus how much reaches nearby coral colonies.

Future work will involve a more thorough investigation of the effect of lagoon morphology on water and coral Mn concentrations. Special care must therefore be taken when analyzing coral Mn/Ca records from different time periods and climate states when certain sites likely experienced significant differences in lagoon morphology and depth. For example, at inhabited atolls, lagoon bathymetry may have looked very different prior to the start of active channel dredging, which could have led to different porewater/seawater Mn(II) and thus coral Mn/Ca signatures. Nevertheless, with demonstrated sea level stability in this region over the past 5,000 years (Woodroffe et al., 2012), there is the exciting potential to expand Mn/Ca-based wind reconstruction further back in time using the extensive sub-fossil coral colonies at Kiritimati and other nearby sites (Grothe et al., 2019), particularly after the impact of diagenesis on the Mn/Ca proxy is thoroughly investigated.

6. SUMMARY AND CONCLUSIONS

In this study, we examined in detail the coral Mn/Ca-based trade-wind indicator and the step-wise transformation of Mn between reservoirs at Kiritimati. As Mn is transferred among water, sediment, and porewater in this complex atoll system, it changes its form to one more favorable for uptake during coral calcification. Initially, insoluble Mn(IV) (from dust) settles through the water column of the lagoon and is buried in the sediments, where it is reduced by organic matter oxidation to its dissolved Mn (II) form. This process, combined with the upward diffusion of Mn(II) from deeper sediments and ample recharge time, allows Mn(II) to accumulate in the porewater reservoir. This Mn(II)-enriched porewater is resuspended into the overlying water column during WWEs whose strength and fetch are sufficient to drive mixing that reaches the sediment–water interface, thereby elevating the Mn(II) concentration of the water, and the Mn content of corals. While the water Mn(II) concentration of Kiritimati's lakes was originally thought to play the role of an analog for the water Mn(II) concentration of the main lagoon prior to wind-driven mixing, the evaporative nature of the lakes, paired with the presence of algal mats (high organic matter content, trapping effect) precludes this comparison. The geochemical analysis of the lake system's Mn reservoirs is, however, instructive for our understanding of the porewater Mn(II) accumulation and mixing depth (i.e., depth of redox transition zone). Our analysis of the behavior of the coral Mn/Ca-wind mechanism's individual components at Kiritimati and Tarawa suggests that overall, the mechanism functions in a similar manner at both locales. The differences between Mn reservoirs at the two islands can be attributed to a) differences in lagoon depth, which affect the reach of wind-driven mixing and b) timing of core collection relative to WWEs, which together determine how much Mn(II) is available to be tapped from sediment porewater. Future work at Kiritimati will involve geochemical analysis of dust collected in previously-deployed traps so that we can quantify dust flux, measure manganese concentration, and determine the source region of dust. Knowledge of these dust properties, as well as the relevant dust mobilization and deposition schemes in the region, will help us further constrain the spatial extent of where this proxy can be used to reconstruct trade-wind variability.

While examining Kiritimati's Mn reservoirs, we also discovered the temporally and spatially variable nature of dissolved Mn(II) in lagoon and lake water. Temporal variability of lagoon Mn(II) demonstrates that precipitation does not have a pronounced affect on lagoon water chemistry, suggesting that it is the westerly wind behavior, rather than precipitation, associated with El Niño events that elevates lagoon Mn(II) content. An in-depth look at the spatial variability of Mn(II) in lagoon water at Kiritimati suggests that the morphology of the lagoon (funneling to a narrow mouth) may partially modulate the amount of Mn(II) that reaches nearby corals. A critical next step in the investigation of this proxy's mechanism is therefore to analyze coral Mn/Ca records from other eligible islands with

diverse lagoon morphologies and varying depths. Future work includes analyzing corals from Abaiang atoll, another island in the Gilbert Islands chain located just 10 km north of Tarawa atoll, which has a lagoon mouth that consists of a series of narrow channels connecting the lagoon to the open ocean, much like Kiritimati.

Armed with a more detailed understanding of the dynamics of Mn at Kiritimati, our findings suggest that the coral Mn/Ca-based trade-wind indicator can be applied to corals from many other sites in the equatorial Pacific to reliably reconstruct trade-wind behavior in the past. These reconstructions will extend beyond the current reach of historical wind records and will capture key WWEs that provide insight on El Niño characteristics. Such a comprehensive wind record will enable the analysis and prediction of interannual and decadal climate variability in a warming world.

Declaration of Competing Interest

The authors declare that they have no known competing financial interests or personal relationships that could have appeared to influence the work reported in this paper.

ACKNOWLEDGEMENTS

Funding and support were provided by NSF OCE-1702130 awarded to DMT and JEC. Fieldwork in Kiritimati was conducted with the support of the Government of Kiribati's Ministry of Environment Lands and Agricultural Development and the Ministry of Fisheries and Marine Resources Development, under Environmental Licenses 011/18 and 008/19 and Research Consent Certificates to DMT.

We acknowledge the Global Tropical Moored Buoy Array Project Office of NOAA/PMEL for the TAO/TRITON buoy daily zonal wind data. We thank B. Koffman for her help in collecting water samples at Kiritimati in January 2020. We thank Tiito Teabi for collecting seawater samples in 2016, and Otea Ioteba for collecting weekly seawater samples from 2018-2019, and again in 2020-2021. We thank Mr. Teratau, Peter Kaitama, and Ann Burentia for their assistance in expediting permits. We thank J. Quade, A. Cohen, and J. Yin for their feedback on the manuscript. We thank Editor-in-Chief J. Catalano and Associate Editor D. Sinclair for coordinating the review process, and three anonymous reviewers for their constructive comments, which greatly improved the manuscript.

APPENDIX A. SUPPLEMENTARY MATERIAL

Supplementary data to this article can be found online at https://doi.org/10.1016/j.gca.2022.04.030.

REFERENCES

Anderson A., Wallin P., Martinsson-Wallin H., Fankhauser B. and Hope G. (2000) Towards a first prehistory of Kiritimati (Christmas) Island, Republic of Kiribati. *J. Polyn. Soc.* **109**, 273–293.

Arfi R., Guiral D. and Bouvy M. (1993) Wind induced resuspension in a Shallow Tropical Lagoon. *Estuar. Coast. Shelf Sci.* **36**, 587–604.

Arp G., Helms G., Karlinska K., Schumann G., Reimer A., Reitner J. and Trichet J. (2012) Photosynthesis versus exopolymer degradation in the formation of microbialites on the Atoll of Kiritimati, Republic of Kiribati, Central Pacific. *Geomicrobiol. J.* **29**, 29–65.

Arthur C. and Woolf M. (2013) Assessment of Tropical Cyclone Risk in the Pacific Region: Technical Report. *Geoscience Australia*, 1–48.

Boyle J. (2001) Redox remobilization and the heavy metal record in lake sediments: a modelling approach. *J. Paleolimnol.* **26**, 423–431.

Burdige D. J. (1993) The biogeochemistry of manganese and iron reduction in marine sediments. *Earth Sci. Rev.* **35**, 249–284.

Carper G. L. and Bachmann R. W. (1984) Wind Resuspension of Sediments in a Prairie Lake. *Can. J. Fish. Aquat. Sci.* **41**, 1763–1767.

Chen D., Lian T., Fu C., Cane M. A., Tang Y., Murtugudde R., Song X., Wu Q. and Zhou L. (2015) Strong influence of westerly wind bursts on El Niño diversity. *Nat. Geosci.* **8**, 339–345.

Chen G. and Wu J. (2019) Meridional distribution of dissolved manganese in the tropical and equatorial pacific. *Geochim. Cosmochim. Acta* **263**, 50–67.

Chen M., Conroy J. L., Sanford R. A., Chee-Sanford J. C. and Connor L. M. (2021) Interpreting lacustrine bulk sediment ^{15}N values using metagenomics in a tropical hypersaline lake system. *J. Paleolimnol.* **65**, 151–168.

Chiodi A. M. and Harrison D. E. (2017) Simulating ENSO SSTAs from TAO/TRITON Winds: The Impacts of 20 Years of Buoy Observations in the Pacific Waveguide and Comparison with Reanalysis Products. *J. Clim.* **30**, 1041–1059.

Delcroix T., Eldin G., McPhaden M. and Morliére A. (1993) Effects of westerly wind bursts upon the western equatorial Pacific Ocean, February–April 1991. *J. Geophys. Res.* **98**, 16379–16385.

Eisenman I., Yu L. and Tziperman E. (2005) Westerly Wind Bursts: ENSO's Tail Rather than the Dog? *J. Climate* **18**, 5224–5238.

England M. H., McGregor S., Spence P., Meehl G. A., Timmermann A., Cai W., Gupta A. S., McPhaden M. J., Purich A. and Santoso A. (2014) Recent intensification of wind-driven circulation in the Pacific and the ongoing warming hiatus. *Nat. Clim. Chang.* **4**, 222–227.

Fedorov A. V., Hu S., Lengaigne M. and Guilyardi E. (2015) The impact of westerly wind bursts and ocean initial state on the development, and diversity of El Niño events. *Clim. Dyn.* **44**, 1381–1401.

Freeman E., Woodruff S. D., Worley S. J., Lubker S. J., Kent E. C., Angel W. E., Berry D. I., Brohan P., Eastman R., Gates L., Gloeden W., Ji Z., Lawrimore J., Rayner N. A., Rosenhagen G. and Smith S. R. (2017) ICOADS Release 3.0: a major update to the historical marine climate record: ICOADS R3.0: A MAJOR UPDATE. *Int. J. Climatol.* **37**, 2211–2232.

Froelich P. N., Klinkhammer G. P., Bender M. L., Luedtke N. A., Heath G. R., Cullen D., Dauphin P. and Blaynehartman D. H. (1978) Early oxidation of organic matter in pelagic sediments of the eastern equatorial Atlantic: suboxic diagenesis. *Geochim. Cosmochim. Acta* **43**, 1075–1090.

Giese B. S. and Harrison D. E. (1991) Eastern equatorial Pacific response to three composite westerly wind types. *J. Geophys. Res.* **96**, 3239–3248.

GoogleMaps and Terrametrics (2020) Google Maps.

Gordon G., Lyons T., Arnold G., Roe J., Sageman B. and Anbar A. (2009) When do black shales tell molybdenum isotope tales? *Geology* **37**, 535–538.

Gounot A. M. (1994) Microbial oxidation and reduction of manganese: Consequences in groundwater and applications. *FEMS Microbiol. Rev.* **14**, 339–349.

Grothe P. R., Cobb K. M., Liguori G., Di Lorenzo E., Capotondi A., Lu Y., Cheng H., Edwards R. L., Southon J. R., Santos G. M., Deocampo D. M., Lynch-Stieglitz J., Chen T., Sayani H. R., Thompson D. M., Conroy J. L., Moore A. L., Townsend K., Hagos M., O'Connor G. and Toth L. T. (2019) Enhanced El Niño-Southern Oscillation variability in recent decades. *Geophys. Res. Lett.* **46**, e2019GL083906.

Hach (2016) pH/ORP Data Sheet, *Tech. rep.*

Harrison D. E. and Giese B. S. (1988) Remote westerly wind forcing of the eastern equatorial Pacific; Some model results. *Geophys. Res. Lett.* **15**, 804–807.

Harrison D. E. and Vecchi G. A. (1997) Westerly Wind Events in the Tropical Pacific, 1986–95. *J. Clim.* **10**, 3131–3156.

Hartten L. M. (1996) Synoptic settings of westerly wind bursts. *J. Geophys. Res. Atmos.* **101**, 16997–17019.

Heiri O., Lotter A. F. and Lemcke G. (2001) Loss on ignition as a method for estimating organic and carbonate content in sediments: reproducibility and comparability of results. *J. Paleolimnol.* **25**, 101–110.

Higley M. C. and Conroy J. L. (2019) The hydrological response of surface water to recent climate variability: A remote sensing case study from the central tropical Pacific. *Hydrol. Process.* **33**, 2227–2239.

Higley M. C., Conroy J. L. and Schmitt S. (2018) Last Millennium Meridional Shifts in Hydroclimate in the Central Tropical Pacific. *Paleoceanogr. Paleoclimatol.* **33**, 354–366.

Inoue M., Ishikawa D., Miyaji T., Yamazaki A., Suzuki A., Yamano H., Kawahata H. and Watanabe T. (2014) Evaluation of Mn and Fe in coral skeletons (Porites spp.) as proxies for sediment loading and reconstruction of 50 yrs of land use on Ishigaki Island, Japan. *Coral Reefs* **33**, 363–373.

Kalnay E., Kanamitsu M., Kistler R., Collins W., Deaven D., Gandin L., Iredell M., Saha S., White G., Woollen J., Zhu Y., Chelliah M., Ebisuzaki W., Higgins W., Janowiak J., Mo K., Ropelewski C., Wang J., Leetmaa A., Reynolds R., Jenne R. and Joseph D. (1996) The NCEP/NCAR 40-Year Reanalysis Project. *Bull. Am. Meteorol. Soc.* **77**, 437–471.

Kessler W. S., McPhaden M. J. and Weickmann K. M. (1995) Forcing of intraseasonal Kelvin waves in the equatorial Pacific. *J. Geophys. Res.* **100**, 10613–10631.

Klinkhammer G. P. and Bender M. L. (1980) The Distribution of Manganese in the Pacific Ocean. *Earth Planet. Sci. Lett.* **46**, 361–384.

Knutson D. W., Buddemeier R. W. and Smith S. V. (1972) Coral Chronometers: Seasonal Growth Bands in Reef Corals. *Science* **177**, 270–272.

Landing W. M. and Bruland K. W. (1980) Manganese in the North Pacific. *Earth Planet. Sci. Lett.* **49**, 45–56.

Lewis S. E., Lough J. M., Cantin N. E., Matson E. G., Kinsley L., Bainbridge Z. T. and Brodie J. E. (2018) A critical evaluation of coral Ba/Ca, Mn/Ca and Y/Ca ratios as indicators of terrestrial input: New data from the Great Barrier Reef, Australia. *Geochim. Cosmochim. Acta* **237**, 131–154.

Lough J. M. (2010) Climate records from corals. *WIREs Climate Change* **1**, 318–331.

Madden R. A. (1986) Seasonal Variations of the 40–50 Day Oscillation in the Tropics. *J. Atmos. Sci.* **43**, 3138–3157.

Madden R. A. and Julian P. R. (1971) Detection of a 40–50 Day Oscillation in the Zonal Wind in the Tropical Pacific. *J. Atmos. Sci.* **28**, 702–708.

McGregor H. V., Woodroffe C., Fischer M., Gagen M. and Fink D. (2013) Coral microatoll reconstructions of El Niño-Southern Oscillation: New windows on seasonal and interannual processes. *PAGES news* **21**, 52–53.

Miller A. and Wu J. (1998) NASS-5 Seawater Reference Material for Trace Metals. *Certified Reference Material*. National Research Council Canada.

Morrison R. and Woodroffe C. D. (2009) The Soils of Kiritimati (Christmas) Island, Kiribati, Central Pacific: New Information and Comparison with Previous Studies. *Pac. Sci.* **63**, 397–411.

National Research Council of Canada (2010a) CASS-5 Nearshore seawater reference material for trace metals.

National Research Council of Canada (2010b) SLEW-3: Estuarine water reference material for trace metals.

Pakhomova S. V., Hall P. O., Kononets M. Y., Rozanov A. G., Tengberg A. and Vershinin A. V. (2007) Fluxes of iron and manganese across the sediment–water interface under various redox conditions. *Mar. Chem.* **107**, 319–331.

Rodellas V., Cook P. G., McCallum J., Andrisoa A., Meule S. and Stieglitz T. C. (2020) Temporal variations in porewater fluxes to a coastal lagoon driven by wind waves and changes in lagoon water depths. *J. Hydrol.* **581**, 124363.

rp5.ru R. P. (2020) rp5.ru reliable prognosis.

Saenger C., Miller M., Smittenberg R. H. and Sachs J. P. (2006) A physico-chemical survey of inland lakes and saline ponds: Christmas Island (Kiritimati) and Washington (Teraina) Islands, Republic of Kiribati. *Aquat. Biosyst.* **2**.

Saha N., Webb G. E., Zhao J. X., Nguyen A. D., Lewis S. E. and Lough J. M. (2019) Coral-based high-resolution rare earth element proxy for terrestrial sediment discharge affecting coastal seawater quality, Great Barrier Reef. *Geochim. Cosmochim. Acta* **254**, 173–191.

Sayani H. R., Thompson D. M., Carilli J. E., Marchitto T. M., Chapman A. U. and Cobb K. M. (2021) Reproducibility of Coral Mn/Ca-Based Wind Reconstructions at Kiritimati Island and Butaritari Atoll. *Geochem. Geophys. Geosyst.* **22**, 1–12.

Schmitt S., Conroy J. L., Flynn T. M., Sanford R. A., Higley M. C., Chen M. and Fouke B. W. (2019) Salinity, microbe and carbonate mineral relationships in brackish and hypersaline lake sediments: A case study from the tropical Pacific coral atoll of Kiritimati. *Depositional Rec.* **5**, 212–229.

Schneider D., Arp G., Reimer A., Reitner J. and Daniel R. (2013) Phylogenetic Analysis of a Microbialite-Forming Microbial Mat from a Hypersaline Lake of the Kiritimati Atoll, Central Pacific. *PLoS ONE* **8**, e66662.

Schoonmaker J., Tribble G., Smith S. and Mackenzie F. (1985) Geochemistry of saline ponds, Kiritimati (Republic of Kiribati). *Proc. Fifth Int. Coral Reef Congress, Tahiti* **3**, 439–444.

Seeberg-Elverfeldt J., Schluter M., Feseker T. and Kölling M. (2005) Rhizon sampling of porewaters near the sediment-water interface of aquatic systems: Rhizon porewater sampling. *Limnol. Oceanogr. Methods* **3**, 361–371.

Seiki A., Takayabu Y. N., Yasuda T., Sato N., Takahashi C., Yoneyama K. and Shirooka R. (2011) Westerly wind bursts and their relationship with ENSO in CMIP3 models. *J. Geophys. Res.* **116**, D03303.

Shen G. and Sanford C. (1990) Trace Element Indicators of Climate Variability in Reef-Building Corals. *Elsevier Oceanogr. Ser.* **52**, 255–283.

Shen G. T. (1993) Reconstruction of El Nino History from Reef Corals. *Bull. Inst. Fr. Etudes Andines* **22**, 125–158.

Shen G. T. and Boyle E. A. (1988) Determination of lead, cadmium and other trace metals in annually-banded corals. *Chem. Geol.* **67**, 47–62.

Shen G. T., Campbell T. M., Dunbar R. B., Wellington G. M., Colgan M. W. and Glynn P. W. (1991) Paleochemistry of

manganese in corals from the Galapagos Islands. *Coral Reefs* **10**, 91–100.

Shen G. T., Linn L. J., Campbell T. M., Cole J. E. and Fairbanks R. G. (1992) A chemical indicator of trade wind reversal in corals from the western tropical Pacific. *J. Geophys. Res.* **97**, 12689–12697.

Shi L., Alves O., Hendon H. H., Wang G. and Anderson D. (2009) The Role of Stochastic Forcing in Ensemble Forecasts of the 1997/98 El Niño. *J. Climate* **22**, 2526–2540.

Shotbolt L. (2010) Pore water sampling from lake and estuary sediments using Rhizon samplers. *J. Paleolimnol.* **44**, 695–700.

Statham P. and Chester R. (1988) Dissolution of manganese from marine atmospheric particulates into seawater and rainwater. *Geochim. Cosmochim. Acta* **52**, 2433–2437.

Statham P., Yeats P. and Landing W. (1998) Manganese in the eastern Atlantic Ocean: processes influencing deep and surface water distributions. *Mar. Chem.* **61**, 55–68.

Sunda W. G. and Huntsman S. A. (1994) Photoreduction of manganese oxides in seawater. *Mar. Chem.* **46**, 133–152.

Sunda W. G., Huntsman S. A. and Harvey G. R. (1983) Photoreduction of manganese oxides in seawater and its geochemical and biological implications. *Nature* **301**, 234–236.

Szpak P., Metcalfe J. Z. and Macdonald R. A. (2017) Best practices for calibrating and reporting stable isotope measurements in archaeology. *J. Archaeol. Sci. Rep.* **13**, 609–616.

Tebo B. M. (1991) Manganese(II) oxidation in the suboxic zone of the Black Sea. *Deep Sea Res. I: Oceanogr. Res. Pap.* **38**, S883–S905.

Thompson D. M. (2022) Environmental records from coral skeletons: A decade of novel insights and innovation. *WIREs Climate Change* **13**, e745.

Thompson D. M., Cole J. E., Shen G. T., Tudhope A. W. and Meehl G. A. (2015) Early twentieth-century warming linked to tropical Pacific wind strength. *Nat. Geosci.* **8**, 117–121.

Valencia M. J. (1977) Christmas Island (Pacific Ocean): Reconnaissance Geologic Observations. *Atoll Res. Bull.* **197**, 1–19.

Vecchi G. A. and Harrison D. E. (2000) Tropical Pacific Sea Surface Temperature Anomalies, El Niño, and Equatorial Westerly Wind Events. *J. Clim.* **13**, 1814–1830.

Verbickas S. (1998) Westerly wind bursts in the tropical Pacific. *Weather* **53**, 282–284.

Woodroffe C. D. and McLean R. F. (1998) Pleistocene morphology and Holocene emergence of Christmas (Kiritimati) Island, Pacific Ocean. *Coral Reefs* **17**, 235–248.

Woodroffe C. D., McGregor H. V., Lambeck K., Smithers S. G. and Fink D. (2012) Mid-Pacific microatolls record sea-level stability over the past 5000 yr. *Geology* **40**, 951–954.

Wyman D. A., Conroy J. L., Osburn M. R. and Atwood A. R. (2021) Coeval Drying Across the Central Tropical Pacific Over the Last Millennium. *Paleoceanogr. Paleoclimatol.* **36**, e2021PA004311.

YSI Incorporated (2018) YSI Professional Plus Multiparameter Water Quality Instrument Spec Sheet, W14-05.

Associate editor: Daniel Sinclair